K-shell ionization cross sections of Al, Si, S, Ca, and Zn for oxygen ions in the energy range 1.1–8 MeV

M. Geretschläger
Institut für Experimentalphysik, Johannes-Kepler-Universität Linz, A-4040 Linz, Austria

Ž. Šmit
J. Stefan Institute, E. Kardelj-University, Ljubljana, Slovenia

E. Steinbauer
Institut für Experimentalphysik, Johannes-Kepler-Universität Linz, A-4040 Linz, Austria

(Received 2 July 1991)

K-shell ionization cross sections induced by 1.1–8-MeV oxygen ions in Al, Si, S, Ca, and Zn were measured using different target thicknesses. The cross sections for vanishingly thin and for charge-equilibrium targets were obtained by extrapolation. The experimental results are compared to the perturbed stationary-state approximation with energy-loss, Coulomb, and relativistic corrections (ECPSSR) cross sections [Brandt and Lapicki, Phys. Rev. A **23**, 1717 (1981)], to the modification of the ECPSSR theory (MECPSSR) [Benka, Geretschläger, and Paul, J. Phys. (Paris) Colloq. Suppl. **12**, C9-251 (1987)], to the theory for direct Coulomb ionization of the $1s\sigma$ molecular orbital [Montenegro and Sigaud, J. Phys. B **18**, 299 (1985)], and to several semiclassical approximation codes using either the united atom binding procedure or the variational approach of Andersen *et al.* [Nucl. Instrum. Methods **192**, 79 (1982)]. The cross sections were also compared to the statistical molecular-orbital theory of inner-shell ionization for (nearly) symmetric atomic collisions [Mittelman and Wilets, Phys. Rev. **154**, 12 (1967)]. For fast collisions ($\xi \sim 1$), the ionization cross sections are well reproduced by theories for direct Coulomb ionization. For slower collisions ($\xi < 1$), the experimental cross sections are systematically higher than the direct-ionization values, but they agree satisfactorily with the summed cross sections for direct Coulomb ionization and for molecular-orbital ionization. Best agreement (within a factor of 2) was found for the sums of MECPSSR and statistical cross sections.

PACS number(s): 34.50.Fa

I. INTRODUCTION

Ionization of *K*-shell electrons by ion impact is dominated by two main mechanisms which depend on the collision symmetry (i.e., the ratio of projectile and target atomic numbers, Z_1/Z_2), and on the scaled projectile velocity v_1/v_{2k} (where v_1 is the projectile velocity and v_{2K} is the *K*-electron velocity of the target atom [1]). For asymmetric collisions ($Z_1/Z_2 \ll 1$) where $v_1/v_{2K} > 1$, target *K* electrons may be treated as independent particles, and first-order theories with screened hydrogenic wave functions may be applied. Furthermore, second-order corrections, e.g., corrections for binding, for Coulomb deflection, and for relativistic motion of the target electrons, make these theories also applicable to more symmetric and to slower collisions. On the other hand, ionization in collisions where $Z_1/Z_2 \simeq 1$ may be described by electron promotion between transient quasimolecular orbitals [2]. For very slow collisions ($v_1/v_2 \ll 1$), ionization can be understood [3] as the Coulomb ionization of molecular orbitals due to the slow passage of the two nuclei past each other and can again be approached by first-order theories but using wave functions of the united atom.

It is interesting to find those regions in $(Z_1/Z_2, v_1/v_{2K})$ space where particular ionization mechanisms predominate. For this purpose, one needs to know cross sections close to the boundaries of particular regions. In a previous paper [4] we measured *K*-shell ionization cross sections of several elements between Si and Ga induced by 1–6.4-MeV carbon ions. We found that the perturbed stationary-state approximation with energy-loss, Coulomb, and relativistic corrections (ECPSSR) of Brandt and Lapicki [5] describes only the high-velocity part of the measurements well. A recent modification of the ECPSSR theory [6] (MECPSSR), which takes formation of molecular orbitals during very slow collisions into account, was found suitable both at high and at low velocities. For medium velocities ($0.15 \leq v_1/v_{2K} \leq 0.25$) and for $Z_1/Z_2 \geq 0.4$, a strong contribution of electron promotion to the ionization cross section was observed. This contribution was found to be well described by the statistical-diffusion model of Mittelman and Wilets [7] (MW).

In the present investigation, we used targets with roughly the same Z_2 values (Al, Si, S, Ca, Zn), but we chose oxygen ions in order to get farther into the region where the statistical model is applicable. Since it is well known that the cross sections depend on the charge state of the projectiles and, hence, on the target thickness

[8–11], we measured the cross sections for several target thicknesses between 1 and 100 $\mu g/cm^2$ and we deduced the limiting values for infinitely thin and for infinitely thick targets by extrapolation. The corresponding ionization cross sections were then compared to the theories.

II. EXPERIMENT

We measured the spectra of x rays and the spectra of backscattered particles simultaneously and we normalized the x-ray yield to the yield of backscattered particles using elastic scattering cross sections corrected for atomic screening effects [12] following the prescription of Andersen *et al.*

A Model No. 5SDH tandem accelerator, manufactured by National Electrostatic Corporation, provided oxygen ions of 1.1–8.0 MeV with charge states from 1+ to 4+. The energy of the ion beam was determined by means of a 90° analyzing magnet which was calibrated with an accuracy of 0.3%. For this energy calibration we use the $^{19}F(p,\alpha\gamma)^{16}O$ resonances between 340.5 and 1372.4 keV and the $^{16}O(\alpha,\alpha)^{16}O$ scattering resonance [13] at 3.045 MeV. In addition, we used the relative-calibration methods described earlier [14]. The ion beam was collimated by a stainless-steel aperture of 1.5-mm diameter mounted 8 cm from the target. Particle currents at the target were typically from 40 to 400 nA.

We prepared our targets by evaporating Al, Si, ZnS, and CaF_2 onto thin ($\sim 15\ \mu g/cm^2$) self-supporting carbon foils. For every element, we prepared targets of different thicknesses, ranging from 1 to 100 $\mu g/cm^2$. The average target thickness was measured by means of a calibrated quartz thickness monitor with an accuracy of 10%.

The x rays were measured using a Si(Li) detector at an angle of 150° with respect to the incoming ion beam. The energy resolution for the Mn $K\alpha$ line was 180 eV full width at half maximum (FWHM). An absorber foil was used between target and detector in order to attenuate the L x rays and to prevent backscattered energetic ions from reaching the detector. The thickness of this absorber foil was calculated from the measured attenuation factors for proton-induced K x rays. (X rays induced by protons are hardly affected by multiple ionization, and the energies are therefore well defined.) To evaluate our x-ray spectra, we used the intrinsic photopeak efficiency ϵ_p obtained as a product of the x-ray absorption probability [15]

$$\epsilon_a = \exp(-\mu_{Be} t_{Be}) \exp(-\mu_{Au} t_{Au}) [1 - \exp(\mu_{Si} t_{Si})]$$

and of the ratio r (photopeak counts to total counts) in K x-ray spectra. Here μ and t are the absorption coefficients and thicknesses of the beryllium window, gold front contact, and silicon sensitive layer, respectively. The ratio r had been determined earlier as a function of x-ray energy [15]. The absorption probability of the Si(Li) detector was determined by measuring the proton-induced x-ray yield simultaneously with the Si(Li) detector and with a surface barrier detector which was calibrated using a method proposed earlier [16]. From the calibration data, the photopeak efficiency and foil transmission were calculated for each projectile energy used. This was necessary because of the energy shift of K x rays due to multiple ionization. Areas and effective energies of the photopeaks were determined using a program [17] that fits Gaussian peaks with exponential and/or polynomial background to the experimental x-ray spectra.

The spectra of elastically backscattered ions were measured by a silicon surface barrier detector. Two geometries were used. For impact energies $E \leq 2.2$ MeV, the detector was positioned at an angle of 90° with respect to the incoming beam. For higher energies, the angle was 156°. The solid angle of the surface barrier detector was defined by means of a stainless-steel aperture. Since the energy calibration curve of the surface barrier detector is rather nonlinear due to the energy-dependent energy loss of ions in the detector window, we carefully determined this curve from the high-energy edges of all measured backscattering spectra. The number of backscattered ions and the energy loss of ions within the targets were determined assuming a linear background due to multiple scattering.

III. X-RAY PRODUCTION CROSS SECTIONS

The x-ray production cross sections were determined using an iterative evaluation procedure described earlier [18]. The energy loss of ions within the targets required for this procedure was deduced from the backscattering spectra for target thicknesses $t \geq 10\ \mu g/cm^2$. For thinner targets, the energy loss was deduced from the measured target thickness and from the stopping power according to Ziegler [19]. Table I shows the estimated errors of the measured x-ray cross sections.

X-ray production cross sections for all but the lightest ions depend on the charge state [4,8–11] and, thus, as the ions penetrate matter and the initially well-defined charge state is transformed to a charge-state distribution [20], on target thickness. The dependence of the cross sections upon target thickness, normalized to the cross section of the thickest target, is shown in Fig. 1 for Al, where the effect is largest. As can be seen, the x-ray production cross sections for targets thicker than $\simeq 30\ \mu g/cm^2$ are enhanced by about a factor of 2 compared to those of very thin targets. For targets of larger Z_2, this effect is

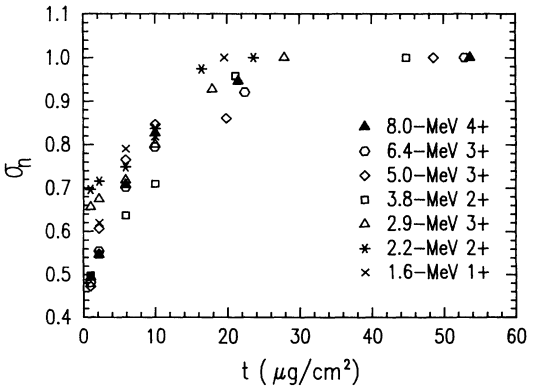

FIG. 1. X-ray production cross sections as a function of average target thickness for oxygen ions on Al, normalized to the value for the thickest target.

TABLE I. Sources of uncertainties in the measured x-ray cross sections.

(a) Individual systematic errors

	Source	Error (%)
X rays	Solid angle	1
	Intrinsic photopeak efficiency	3–7
	Foil absorption	0.5–2
Particles	Solid angle	1,2
	Backscattering angle	0.5
	Bombarding energy	0.3

(b) Total systematic errors

Al	Si	S	Ca	Zn
8%	7%	6%	5%	4%

(c) Nonsystematic errors

Source	Error (%)
X-ray yield[a]	0.5–10
Particle yield[a]	0.5–20
Pileup and deadtime correction	0.1–0.5
Energy loss within the target[b]	1–8

[a]The yield errors are the sum of statistical errors and estimated fit errors.
[b]The energy errors were converted to x-ray errors using theoretical cross sections for ionization (Refs. [5,7]) and scattering (Ref. [12]).

smaller; for Zn, the x-ray production cross sections are essentially independent of the target thickness.

The ions penetrating the target approach their charge-state equilibrium exponentially. To describe the x-ray production cross section (σ_x) as a function of target thickness (t), we used the two-component model of Gray [21]. Since all our incoming ions have filled K shells, Eq. 5.5.23 of Ref. [21] (note an error there) can be simplified to

$$\sigma_x(t)=a-b[1-\exp(-t/t_c)]t_c/t \ .$$

Fitting this function to the data by varying the parameters a, b, and t_c we determined the x-ray production cross sections for both infinitely thin and charge-equilibrium targets: $\sigma_x(0)=a-b$ and $\sigma_x(\infty)=a$, respectively. The results are given in Tables II and III, respectively. Table III also gives the average equilibrium charge $\bar{Q}_e$ obtained from a fit to the values given by Wittkower and Betz [20]. The width of the charge distribution varied from 0.9 to 0.8 elementary charge units for oxygen ion energies from 1 to 8 MeV.

To our knowledge the only comparable data in the literature are those by Laubert and Losonsky [22] for Al. We note that those authors used infinitely thick targets

TABLE II. Experimental x-ray production cross sections (in barns) for oxygen ions of charge state Q on infinitely thin targets. The errors (in %) are given below the values. They include systematic errors, nonsystematic errors, and also the extrapolation errors. Nonsystematic errors and extrapolation errors were added in quadrature. The total systematic errors were added linearly.

E (MeV)	Q	Al	Si	S	Ca	Zn
8.0	4+	5946	3033	791	79.9	3.12
		(15%)	(15%)	(14%)	(12%)	(10%)
6.4	3+	3090	1413	313	28.9	1.32
		(15%)	(15%)	(14%)	(12%)	(11%)
5.0	3+	1572	613	131	9.13	0.483
		(16%)	(16%)	(14%)	(13%)	(12%)
3.8	2+	612	231	38.3	2.51	0.137
		(17%)	(17%)	(16%)	(14%)	(15%)
2.9	3+	258	82.2	13.5	0.819	0.0474
		(19%)	(18%)	(18%)	(16%)	(20%)
2.2	2+	85.3	24.0	3.86	0.264	
		(22%)	(21%)	(20%)	(18%)	
1.6	1+	19.1	5.90	1.05	0.0491	
		(26%)	(25%)	(25%)	(22%)	
1.1	1+	3.72	1.38			
		(30%)	(30%)			

TABLE III. Experimental equilibrium x-ray production cross sections (in barns) for oxygen ions in charge equilibrium $\bar{Q}_e$ on various targets. The errors (in %) are given below the values. They include systematic errors, nonsystematic errors, and extrapolation errors. Nonsystematic errors and extrapolation errors were added in quadrature. The total systematic errors were added linearly.

E (MeV)	$\bar{Q}_e$	Al	Si	S	Ca	Zn
8.0	5.5+	15 240	6846	1328	99.4	3.12
		(15%)	(15%)	(14%)	(12%)	(10%)
6.4	5.1+	7786	3087	659	42.5	1.32
		(15%)	(15%)	(14%)	(12%)	(11%)
5.0	4.8+	3826	1343	240	11.7	0.483
		(16%)	(16%)	(14%)	(13%)	(12%)
3.8	4.4+	1476	435	85.6	3.40	0.137
		(18%)	(18%)	(16%)	(15%)	(15%)
2.9	4.0+	444	122	21.2	1.10	0.0474
		(21%)	(20%)	(19%)	(16%)	(20%)
2.2	3.5+	141	32.5	6.53	0.322	
		(26%)	(23%)	(21%)	(19%)	
1.6	3.0+	43.4	9.03	2.86	0.102	
		(29%)	(27%)	(28%)	(23%)	
1.1	2.5+	9.08	1.51			
		(36%)	(34%)			

for ion energies 1–3 MeV and about 20-μg/cm^2-thick targets (oriented at an angle of 45° with respect to the ion beam) for ion energies of 1–90 MeV. Their infinitely-thick-target data agree with our extrapolated thick-target values within our combined errors. Their "best values," however, are between our thick- and thin-target limit (see Fig. 1) because their "thin targets" were obviously not thin enough.

IV. IONIZATION CROSS SECTIONS

We converted our x-ray production cross sections into ionization cross sections using fluorescence yields ω which are enhanced due to multiple outer-shell ionization. We estimated this enhancement using the measured energy shifts of the K x rays and a procedure which was described before [18]. For Al, Si, and S, we estimated ω from the $K\alpha$ line shift only, since we could not determine $K\beta$ line shifts and intensity ratios of $K\beta$ and $K\alpha$ lines accurately enough. The fluorescence yields thus estimated were larger by factors of 1.15–1.44 than the single-hole values of Krause [23].

A. Infinitely thin targets

The ionization cross sections for infinitely thin targets were compared to the theories for Coulomb ionization (ECPSSR) [5]; MECPSSR [6]; semiclassical approximation (SCA) calculations of Laegsgaard *et al.* [24], of Trautman *et al.* [25] and of Šmit [26]; and predictions of Montenegro and Sigaud [27]) and to the theory for ionization by electron promotion (the statistical-diffusion model of Mittelman and Wilets [7]). The charge states of the incoming ions (see Table II) were $Q \leq 4$ and hence the ions had filled K shells. Therefore, target K-shell to projectile K-shell electron capture could not contribute to the ionization cross section. Contributions due to capture of target K electrons to the projectile L shell are small [28] and we therefore neglected them. Figures 2–6 show the experimental ionization cross sections for infinitely thin targets normalized to theories for Coulomb ionization as a function of the scaled projectile velocity $\xi = 2v_1/(\Theta v_{2K})$, where $\Theta = I_k/(Z_2 - 0.3)^2 R$, with I_k the experimental ionization energy and R the Rydberg constant.

For collision systems with $Z_1/Z_2 \leq 0.4$ (Ca, Zn) the ECPSSR theory [5] (Fig. 2) and the MECPSSR theory [6] (Fig. 3) reproduce the measurements reasonably well. For systems with $Z_1/Z_2 \geq 0.5$ and scaled velocities $\xi \leq 0.9$, both theories predict cross sections too small, and these predictions become even worse with decreasing ξ and increasing Z_1/Z_2. The MECPSSR, which takes into account formation of molecular orbitals at very slow velocities, is not as bad as the ECPSSR at these low velocities, but it is evident that the collision systems $Z_1/Z_2 \geq 0.5$ cannot be described by Coulomb ionization alone for $\xi \leq 0.9$.

In the SCA calculations some approximations are necessary to describe the binding effect. For the SCA calculations according to Laegsgaard *et al.* [24] and accord-

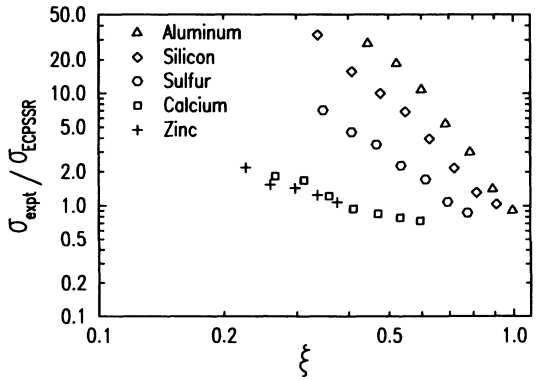

FIG. 2. Experimental ionization cross sections for infinitely thin targets σ_{expt} normalized to ECPSSR cross sections σ_{ECPSSR}.

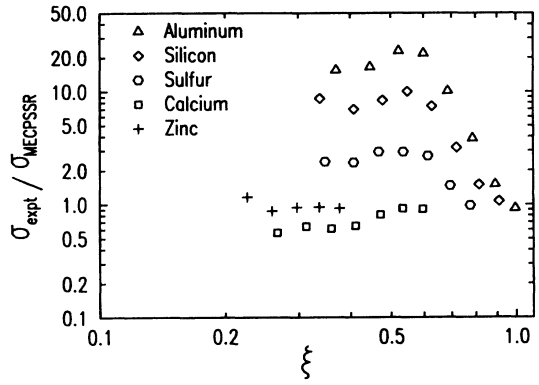

FIG. 3. Experimental ionization cross sections for infinitely thin targets σ_{expt} normalized to MECPSSR cross sections $\sigma_{MECPSSR}$.

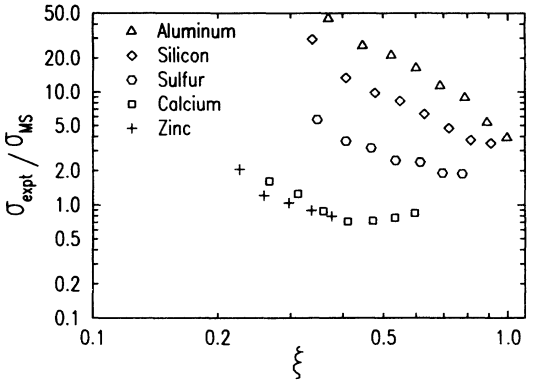

FIG. 6. Experimental ionization cross sections for infinitely thin targets σ_{expt} normalized to the predictions of Montenegro and Sigaud σ_{MS}.

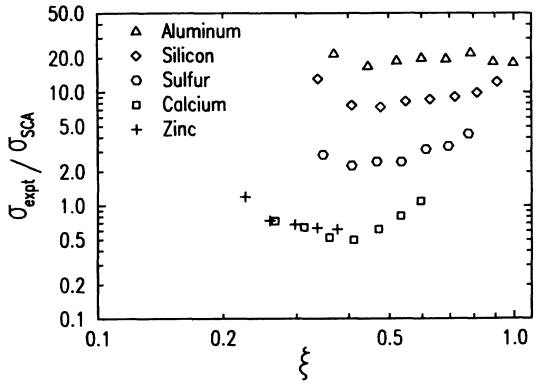

FIG. 4. Experimental ionization cross sections for infinitely thin targets σ_{expt} normalized to SCA cross sections σ_{SCA} due to Refs. [24] and [25], which are indistinguishable in this scale.

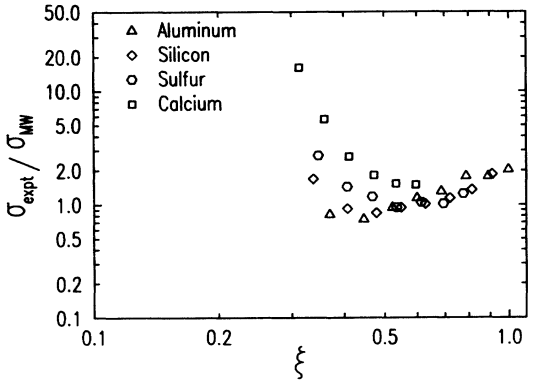

FIG. 7. Experimental ionization cross sections for infinitely thin targets σ_{expt} normalized to the diffusion cross sections of Mittelman and Wilets σ_{MW}.

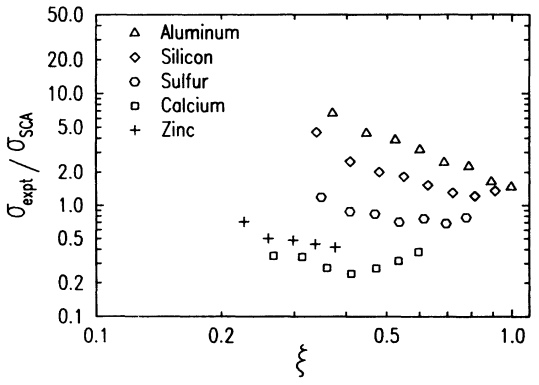

FIG. 5. Experimental ionization cross sections for infinitely thin targets σ_{expt} normalized to the SCA cross sections σ_{SCA} of Ref. [26].

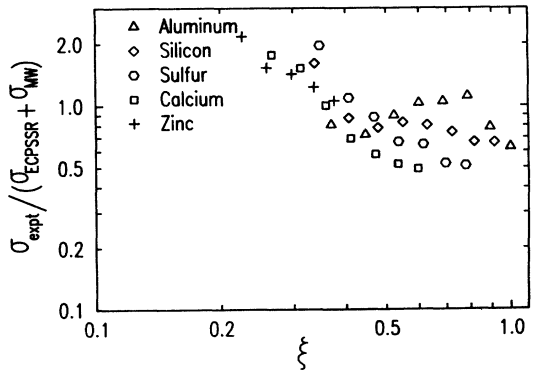

FIG. 8. Experimental ionization cross sections for infinitely thin targets σ_{expt} normalized to the sum of ECPSSR cross sections σ_{ECPSSR} and diffusion cross sections σ_{MW}.

ing to Trautmann and Rösel [25] we used the experimental united atom binding energy. For calculations according to Šmit [26] we used the variational procedure of Andersen *et al.* [29] to calculate an effective binding energy for an average distance projectile-target nucleus. Both the simplified SCA model of Laegsgaard *et al.* [24] and the much more sophisticated numerical calculations of Trautmann and Rösel [25] predict almost identical cross sections for our collision systems (Fig. 4). Both SCA approaches fail, at all velocities, in predicting the experiments for collision systems $Z_1/Z_2 \geq 0.5$. Figure 5 shows a comparison of our measurements to the SCA calculations of Šmit [26]. Obviously, the variational procedure for calculating binding energies gives better values for elements of low Z_2, but overprecits the cross sections for Ca and Zn ($Z_1/Z_2 \leq 0.4$) by about a factor of 3.

Figure 6 shows the comparison of the present cross sections to the prediction of Montenegro and Sigaud [27] (MS), who apply adiabatic perturbation theory to the ionization of $1s\sigma$ molecular orbitals by direct Coulomb interaction and extend the theory to less adiabatic collisions by imposing an asymptotic matching with the semiclassical approximation. For $\xi \leq 0.6$, MS predictions and ECPSSR predictions (Fig. 2) are more or less identical. For $\xi > 0.6$, Montenegro and Sigaud predict significantly smaller cross sections than the ECPSSR.

Figures 2 to 6 show that the MECPSSR predictions are generally closest to the experimental values. But it is obvious that in collision systems with $Z_1/Z_2 \geq 0.4$, K-shell ionization cannot be described by Coulomb ionization alone for scaled velocities $\xi \leq 0.9$.

It is known [30–32] that for $Z_1/Z_2 \geq 0.3$ and $v_1/v_{2K} < 1$, Pauli excitation can contribute significantly to K-shell ionization. We used a statistical treatment of the electron promotion from inner shells into the continuum [7,33,34]. We calculated the sum of K-shell ionization cross sections for the projectile and target atoms using the diffusion model of Mittelman and Wilets [7] and the diffusion constants of Brandt [33]. The K-shell ionization cross sections of the target atoms were then found by multiplying the summed cross sections by the vacancy sharing factor of Meyerhof *et al.* [35], calculated using the ionization energy for oxygen ions in charge state $Q=2$. Figure 7 shows the experimental ionization cross sections normalized to the diffusion cross sections (σ_{MW}). Evidently, these cross sections reproduce the experimental values for collision systems $Z_1/Z_2 \geq 0.5$ within a factor of 2. As we found earlier for carbon ions [4], Pauli excitation contributes most to the cross sections for $0.4 \leq \xi \leq 0.8$.

In Figs. 8–12, we show on an expanded scale the experimental ionization cross sections for infinitely thin targets, normalized to the sum of the predictions for direct Coulomb ionization and for Pauli excitation. These predictions now agree much better with experiments. The sum of MECPSSR and Pauli excitation gives best results, and the deviations from unity have been reduced from the previous factor of 20 to a factor about 1.5. These remaining deviations might be due to uncertainties in the fluorescence yields used and to the uncertainty in the semiempirical diffusion constant. (Note that the semiempirical diffusion constant of Brandt [33] was obtained without distinguishing thin and thick targets.)

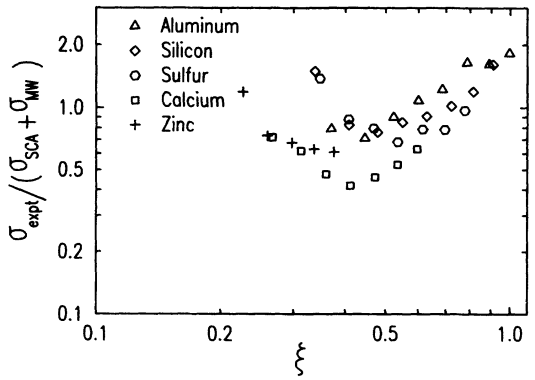

FIG. 10. Experimental ionization cross sections for infinitely thin targets σ_{expt} normalized to the sum of SCA cross sections σ_{SCA} (Refs. [24,25]; see text) and diffusion cross sections σ_{MW}.

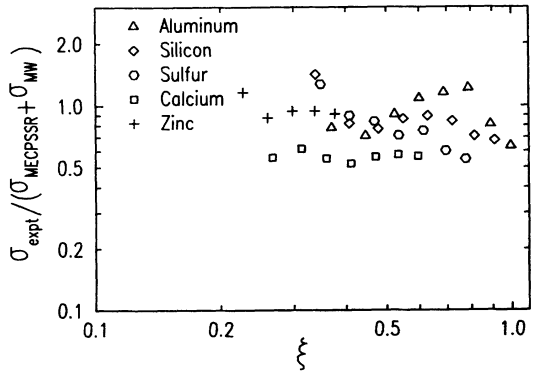

FIG. 9. Experimental ionization cross sections for infinitely thin targets σ_{expt} normalized to the sum of MECPSSR cross sections $\sigma_{MECPSSR}$ and diffusion cross sections σ_{MW}.

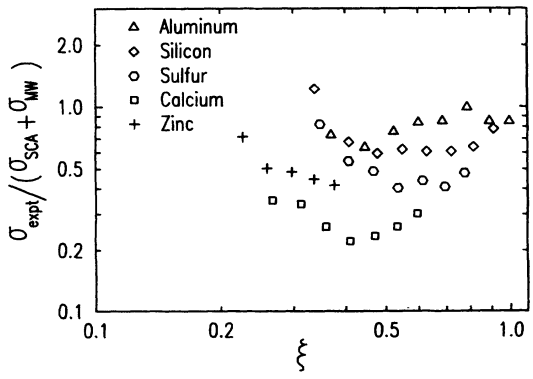

FIG. 11. Experimental ionization cross sections for infinitely thin targets σ_{expt} normalized to the sum of SCA cross sections σ_{SCA} (Ref. [26]) and diffusion cross sections σ_{MW}.

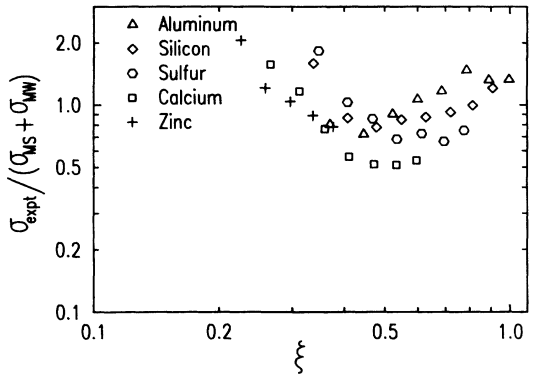

FIG. 12. Experimental ionization cross sections for infinitely thin targets σ_{expt} normalized to the sum of the cross sections of Ref. [28], σ_{MS}, and diffusion cross sections σ_{MW}.

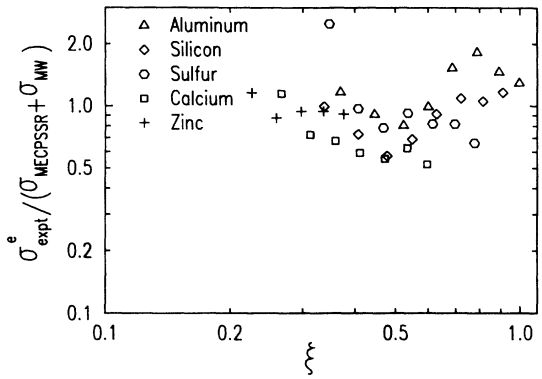

FIG. 13. Experimental equilibrium ionization cross sections σ^e_{expt} normalized to the sum of MECPSSR cross sections σ_{MECPSSR} and diffusion cross sections σ_{MW}.

B. Charge-equilibrium ionization cross sections

The experimental equilibrium ionization cross sections were also compared to the sum of the diffusion cross section and the various cross sections for direct Coulomb ionization as mentioned above. In equilibrium, the ions have a charge distribution described by an average charge $\bar{Q}_e$ and by a width d (see Ref. [20]). Hence, a small fraction of ions have one or even two K holes and contribute to the vacancy production not only by direct ionization but also by K capture. However, electron capture by the projectile is implicitly included in Pauli excitation. To take the various charge states in the diffusion cross sections into account, we calculated the vacancy sharing factor of Meyerhof *et al.*, [35] for oxygen ions having a Gaussian equilibrium charge distribution. We assumed a simple model [4] for the dependence of the oxygen K-shell binding energy upon the ion charge. Averaging over all charge states, we obtained an average vacancy sharing factor and, hence, an average diffusion cross section.

The agreement with the experiments was similar to that obtained for the thin targets. As an example, we show in Fig. 13 the experimental equilibrium ionization cross sections normalized to the sum of MECPSSR and diffusion cross sections. Again, MECPSSR gives best results. The remaining deviations from unity are of similar magnitude as for the thin targets, and are most probably due to the same reasons.

V. CONCLUSION

In the entire parameter range investigated in this work ($0.27 \leq Z_1/Z_2 \leq 0.62$, $0.22 \leq \xi \leq 1$), the experimental cross sections are satisfactorily represented by the sum of the cross sections for statistical and for direct Coulomb ionization. Among several theories tested, best agreement with the experimental values was found using the sum of statistical and MECPSSR cross sections.

For $Z_1/Z_2 \geq 0.5$ (oxygen ions on Al, Si, and S) and $0.3 \leq \xi \leq 1$, interactive level crossing becomes the predominant ionization mechanism for ion-atom collisions. In this region, experimental cross sections are well reproduced by the cross sections according to the statistical model of Mittelman and Wilets [7] alone.

ACKNOWLEDGMENT

One of the authors (Ž.Š.) is indebted to the Johannes Kepler University of Linz for kind hospitality.

[1] D. H. Madison and E. Merzbacher, in *Atomic Inner Shell Processes,* edited by B. Crasemann (Academic, New York, 1975).
[2] U. Fano and W. Lichten, Phys. Rev. Lett. **14**, 627 (1965).
[3] J. S. Briggs, J. Phys. B **8**, L485 (1975).
[4] M. Geretschläger, Ž. Šmit, and O. Benka, Phys. Rev. A **41**, 123 (1990).
[5] W. Brandt, and G. Lapicki, Phys. Rev. A **23**, 1717 (1981).
[6] O. Benka, M. Geretschläger, and H. Paul, J. Phys. (Paris) Colloq. C9-251 (1987).
[7] M. H. Mittelman and L. Wilets, Phys. Rev. **154**, 12 (1967).
[8] T. J. Gray, in *Methods of Experimental Physics,* edited by P. Richard (Academic, New York, 1980), Vol. 17, p. 250.
[9] B. Knaf, G. Presser, and J. Stähler, Z. Phys. A **282**, 25 (1977).
[10] G. Presser, E. Scherer, and J. Stähler, Z. Phys. A **295**, 27 (1980).
[11] H. Tawara, P. Richard, T. J. Gray, P. Pepmiller, J. R. Macdonald, and R. Dillingham, Phys. Rev. A **19**, 2131 (1979).
[12] H. H. Andersen, F. Besenbacher, P. Loftager, and W. Möller, Phys. Rev. A **21**, 1891 (1980).
[13] J. R. Cameron, Phys. Rev. **90**, 839 (1953).
[14] D. Semrad, M. Geretschläger, and A. Rabler, Nucl. Instrum. Methods **215**, 549 (1983).
[15] M. Geretschläger, Nucl. Instrum. Methods B **28**, 289 (1987).
[16] M. Geretschläger, Nucl. Instrum. Methods **192**, 117 (1982).
[17] E. Steinbauer, Ph.D. thesis, Verband der wissenschaftlichen Gesellschaften sterreichs (VWG), A-1070 Wien, 1987 (unpublished).

[18] M. Geretschläger and O. Benka, Phys. Rev. A **34**, 866 (1986).
[19] J. F. Ziegler, Computer program TRIM90.
[20] A. B. Wittkower and H. D. Betz, At. Data Nucl. Data Tables **5**, 113 (1973).
[21] T. J. Gray, in *Methods of Experimental Physics,* edited by P. Richard (Academic, New York, 1980), Vol. 17, p. 264.
[22] R. Laubert and W. Losonsky, Phys. Rev. A **14**, 2043 (1976).
[23] M. O. Krause, J. Phys. Chem. Ref. Data **8**, 307 (1979).
[24] E. Laegsgaard, U. J. Andersen, and M. Lund, in *Proceedings of the Tenth International Conference on the Physics of Electron and Atomic Collisions, Paris, 1977,* edited by G. Watel (North-Holland, Amsterdam, 1977).
[25] D. Trautmann and F. Rösel, FORTRAN Code IONHYD (private communication).
[26] Ž. Šmit, Z. Phys. D (to be published).
[27] E. C. Montenegro and G. M. Sigaud, J. Phys. B **18**, 299 (1985).
[28] G. Lapicki and F. D. McDaniel, Phys. Rev. A **22**, 1896 (1980).
[29] J. U. Andersen, E. Laegsgaard and M. Lund, Nucl. Instrum. Methods **192**, 79 (1982).
[30] U. Fano and W. Lichten, Phys. Rev. Lett. **14**, 627 (1963).
[31] K. Taulbjerg, J. S. Briggs, and J. Vaaben, J. Phys. B **9**, 1351 (1976).
[32] W. E. Meyerhof and K. Taulbjerg, Annu. Rev. Nucl. Sci. **27**, 279 (1977).
[33] W. Brandt and K. W. Jones, Phys. Lett. **57A**, 35 (1976).
[34] W. Brandt, IEEE Trans. Nucl. Sci. **NS-26**, 1179 (1979).
[35] W. E. Meyerhof, R. Anholt, and T. K. Saylor, Phys. Rev. A **16**, 169 (1977).